PCCP

ROYAL SOCIETY OF CHEMISTRY

PAPER

View Article Online
View Journal | View Issue

Cite this: *Phys. Chem. Chem. Phys.*, 2021, **23**, 26178

Novel two-dimensional boron oxynitride predicted using the USPEX evolutionary algorithm†

Zakhar I. Popov, *[a] Kseniya A. Tikhomirova,[ab] Victor A. Demin,[a] Suman Chowdhury,[b] Artem R. Oganov,[b] Alexander G. Kvashnin[b] and Dmitry G. Kvashnin *[ac]

Received 16th August 2021,
Accepted 4th November 2021

DOI: 10.1039/d1cp03754d

rsc.li/pccp

Oxidation is a unique process that significantly changes the structure and properties of a material. Doping of h-BN by oxygen is a hot topic in material science leading to the possibility of synthesis of novel 2D structures with customized electronic properties. It is still unclear how the atomic structure changes in the presence of external atoms during the oxidation of h-BN. We predict novel two-dimensional (2D) arrangements of boron oxynitride using the evolutionary algorithm of crystal structure prediction USPEX. All considered structures demonstrate semiconducting properties with a reduced bandgap compared with h-BN. Both molecular dynamics and phonon calculations show the dynamical stability of the new 2D $B_5N_3O_2$ phase, and our calculations demonstrate that it can form a bulk layered structure with an interlayer distance larger than that of pure h-BN. The optical characterization shows a redshift of the absorption spectrum compared with pure h-BN. Incorporation of oxygen into the structure of 2D BN during synthesis or oxidation can dramatically change the covalent network of h-BN while preserving its two-dimensionality and flatness, following the presence of local dipole moments which could improve the piezoelectric properties.

I. Introduction

Chemically stable BN bulk materials can exist in four different polymorphic modifications: sp^2-hybridized hexagonal (h-BN) and rhombohedral (r-BN), and sp^3-hybridized cubic (c-BN) and wurtzite (w-BN).[1–5] Most promising among technological applications is h-BN[6] which attracts more attention due to its graphite-like layered crystal structure. While B and N atoms are held together by strong covalent bonds densely covering the plane, between BN layers there are only week van der Waals forces. In contrast to graphene, BN has polar B–N bonds. BN nanoplates are known to preserve their thermal stability up to 1000 °C, undergoing oxidation in the range between 1000 and 1200 °C, with the formation of B_2O_3.[7]

From the practical point of view the use of h-BN in electronics is limited by wide band gap of ~5.5 eV.[8–12] Nevertheless, recent reports[7,13] state that oxygen doping of the monolayer h-BN structure leads to reduction of band gap to 2.1 eV together with the observation of intriguing optical (fluorescence) and magnetic properties that depend on defect types. The defect chemistry of h-BN is most likely dominated by defects conditioned by impurities such as carbon, oxygen, and hydrogen. Substitutional carbon and oxygen, as well as interstitial hydrogen and boron vacancy–hydrogen complexes, are known as low-energy defects in h-BN.[14] The structure of oxidized boron nitride is based on the conception that the oxygen atoms incorporated in the h-BN lattice by replacing the nitrogen atoms. Such a way will provide a new practical method to control the electronic and magnetic properties of boron nitride.[6] It was shown by Weng *et al.*[7] that the band gap of h-BN may vary depending on the concentration of oxygen introduced into its crystal structure instead of nitrogen atoms with the maximum oxygen concentration of 23%. This allows to consider new bottom-up synthesis routes and incorporation of two-color fluorescent boron oxynitride nanodots into a hybrid organic–inorganic film.[15] In fact, theoretical modeling confirmed that the band gap of BN nanosheets and BN nanotubes can be significantly reduced by replacement of nitrogen atoms by oxygen atoms.[16,17] Similarly, the optical, electronic, and magnetic properties can be tuned as has been predicted in numerous theoretical works, *i.e.* ref. 17–19. Previous experimental studies using ring dark field scanning transmission microscopy demonstrate that the presence of oxygen atoms in the h-BN lattice is truly possible.[20]

[a] *Emanuel Institute of Biochemical Physics RAS, 4 Kosygin Street, Moscow 119334, Russian Federation. E-mail: zipcool@bk.ru*
[b] *Skolkovo Institute of Science and Technology, Skolkovo Innovation Center, 3 Nobel Street, Moscow, 121025, Russian Federation*
[c] *Moscow Institute of Physics and Technology, Institutsky Pereulok, Dolgoprudny 141701, Moscow Region, Russian Federation. E-mail: dgkvashnin@phystech.edu*

† Electronic supplementary information (ESI) available. See DOI: 10.1039/d1cp03754d

Thus, the oxidized boron nitride could be a promising material for further investigations and applications, because it is still unclear how the atomic structure changes in the presence of external atoms during the oxidation of h-BN. This motivated us to study the crystal structures of B–N–O by using the evolutionary structure prediction of two-dimensional materials.[21]

II. Methods

The search for thermodynamically stable 2D compounds in the B–N–O system was performed using the variable-composition evolutionary search as implemented in the USPEX code.[22–24] The thickness of 2D crystals is restricted in a range of 0–6 Å, and the total number of atoms is specified to be 8–18. The initial population of 180 structures were generated using a random symmetric structure generator,[24] while the subsequent generation contains 120 structures, 20% of which were produced using a random symmetric structure generator, and 80% by variation operators (heredity, soft mutation, and atomic transmutation).

All structures were relaxed using the density functional theory (DFT).[25,26] The generalized gradient approximation (GGA) method was used with the Perdew–Burke–Ernzerhof (PBE) parameterization for the exchange–correlation functional,[27] implemented in the VASP package.[28–31] For bulk structures, van der Waals interactions were taken into account using the Grimme correction.[32] The cutoff energy of plane waves was set to 500 eV. The sampling of the Brillouin zone was done using a uniform k-point grid with a resolution of $2\pi \times 0.5$ Å^{-1}.

To study the stability of the predicted phases, we computed their energy of formation:

$$E_f = \frac{E_{BNO} - n\mu_B - m\mu_N - p\mu_O}{N}$$

where E_{BNO} is the total energy of the predicted structure; μ_B, μ_N, and μ_O are the chemical potentials of atoms calculated for a-B, molecular nitrogen, and oxygen; n, m, and p are the number of boron, nitrogen, and oxygen atoms; and N is the total number of atoms in the system.

The phonon dispersion curves of the predicted structures were calculated using the finite displacement method as implemented in the PHONOPY code.[33]

The extinction coefficient was calculated using the superposition of the Lorentz oscillators to simulate the complex dielectric function depending on the frequency of light. The real part was determined using the Kramers–Kronig relations, the imaginary part was found by summing over the unfilled states.[34] In terms of the dielectric function, the extinction coefficient is

$$K(\lambda) = \left[\frac{\sqrt{\varepsilon_1^2 + \varepsilon_2^2} - \varepsilon_1}{2}\right]^{1/2}$$

We applied the *ab initio* molecular dynamics (AIMD) to the B–N–O structures to study their dynamical and thermal stability using a $2 \times 2 \times 1$ supercell. The molecular dynamics simulations were carried out at constant temperatures of 600 and 1200 K using the Nosé–Hoover thermostat.[35,36] The total time of the simulations was set to 3.5 ps, which is enough to observe critical changes in the atomic structure, with a time step of 1 fs. The atomic structure was recorded after every 10 ionic steps.

III. Results and discussion

Crystal structure prediction

On the basis of the experimental data,[7] the composition of boron nitride nanosheets with oxygen doping (44.7% of boron, 30.7% of nitrogen, 23.1% of oxygen, 1.5% of other impurities) was set as the starting point for structure prediction. We predicted new two-dimensional structures based on h-BN doped by oxygen atoms with the general formula $B_xN_yO_z$, where x, y, and z are the number of boron, nitrogen, and oxygen atoms in the unit cell, respectively. Two types of structures were considered: (i) those with the sum of the N and O atoms equal to the number of the B atoms ($x = y + z$), to simulate ternary systems obtained using the growth mechanism, and (ii) those with an equal number of the B and N atoms ($x = y$), to simulate ternary systems created by oxygen doping of h-BN (Fig. 1a and b).

Fig. 1a shows the case (i) results of the search for B–N–O structures with fixed compositions at different oxygen concentrations. For N-rich structures (*e.g.*, B_3N_4O) with an oxygen concentration of 17%, we obtained a monolayer B_3N_2O structure with separate N_2 molecules near the surface. These results confirm that substitution of B would cause structural deformations and instability of a BN sheet.[16]

It was found that B_4N_3O and B_3N_2O compositions (Fig. 1a) have a structure of h-BN with oxygen replacing some nitrogen atoms. Increasing the oxygen concentration, defined as the number of the oxygen atoms related to the total number of atoms in the B–N–O structure, to 20% ($B_5N_3O_2$) leads to the formation of another structure with 5 to 11 periodically arranged defects along the y axis, which are separated by a line of 6-member rings along the x axis (Fig. 1a). Importantly, the oxygen concentration in $B_5N_3O_2$ is close to that of the experimental composition.[7] To compare the calculation results with the experimental data, we estimated the total energy and interlayer distance in the layered bulk structure of $B_5N_3O_2$ and pure h-BN. The interlayer distance of bulk $B_5N_3O_2$ was found to be larger than that of h-BN (3.42 *vs.* 3.23 Å), which agrees with the experimental data.[7]

Then we applied an evolutionary algorithm to predict the B–N–O compositions with an equal number of boron and nitrogen atoms. Studying the possibility of formation of 2D B–N–O structures *via* oxygen doping of h-BN, we predicted B_3N_3O, B_4N_4O, B_6N_6O, and B_8N_8O compositions using the USPEX algorithm. Fig. 1b shows the geometry of these lowest-energy B_xN_xO (x = 3, 4, 6, 8) nanostructures. Oxidation of h-BN led to formation of 2D materials with unique structures differing from that of h-BN. For clarity, in Fig. 1b the polygons forming unit cells are painted in different colors: n-angle polygons (n = 4, 5, 6, 7, 8,...) are shown in yellow, blue, green, red, orange, and gray, respectively. The structures with a higher

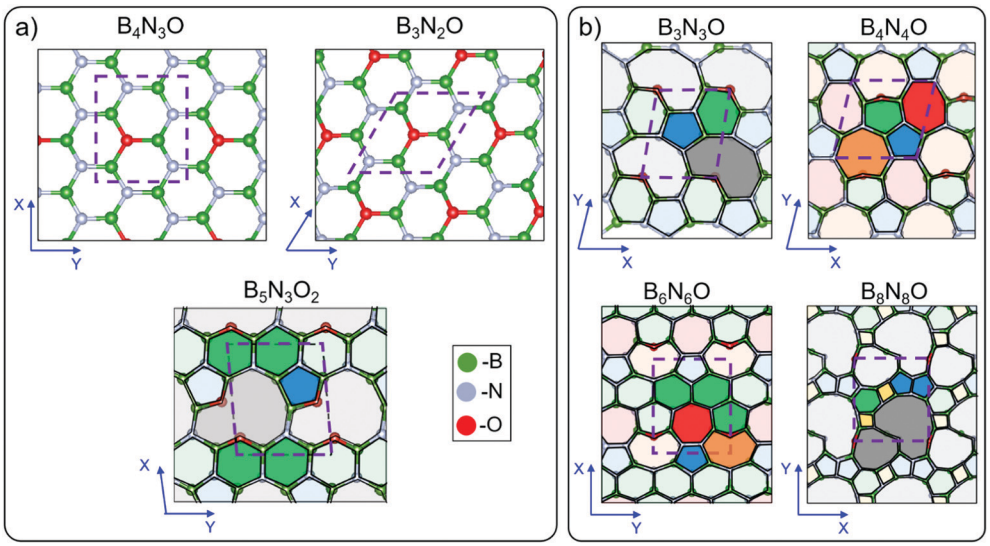

Fig. 1 Predicted $B_xN_yO_z$ structures with (a) $x = y + z$ and (b) $x = y$. The boron, nitrogen, and oxygen atoms are shown in green, gray, and red, respectively.

oxygen concentration, B_3N_3O and B_4N_4O, in addition to 6-member formations also have 5-atom ones with a homoatomic bond between the nitrogen atoms. The oxygen atoms are often located in 6-member rings, which are adjacent to polygons with 8, 9 and larger number of vertices.

To check the stability of the predicted B–N–O structures, we calculated the ternary phase diagram (Fig. 2). Because bulk layered materials always have a lower energy than their 2D counterparts, we used only two-dimensional structures to construct the ternary phase diagram except the elemental structures of boron, oxygen, and nitrogen. For this reason, bulk B_2O_3 was not considered, whereas the structures of two-dimensional stoichiometric boron oxides[37] were taken into account. It was found that the B–N–O structures with an equal number of the boron and nitrogen atoms have the energy of formation about 1.5 times lower in absolute value than the structures with the chemical ratio of $x = y + z$ ($B_5N_3O_2$, B_3N_2O, and B_4N_3O). The $B_5N_3O_2$ structure has the lowest formation energy among all considered 2D B–N–O structures, even in comparison with h-BN, which makes it thermodynamically stable (Fig. 2). Increasing the concentration of oxygen leads to the formation of structures associated with nitrogen-doped boron oxides rather than oxidized boron nitrides.

At low concentrations of oxygen, defective and low-density structures B_6N_6O and B_8N_8O are formed, containing a large variety of polygonal rings in the unit cell, including 4-, 7-, 8-, and 12-member rings interconnected with boron nitride hexagons.

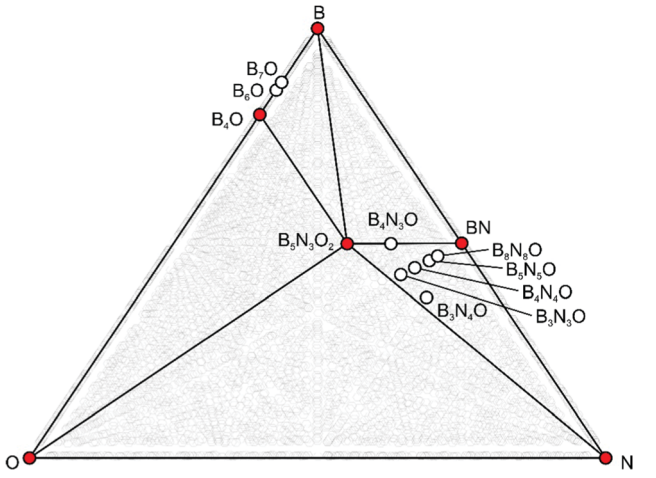

Fig. 2 Ternary phase diagram of the two-dimensional B–N–O structures in the formation energy and composition coordinates. Thermodynamically stable and metastable structures are shown by red and white circles, respectively.

Stability of $B_5N_3O_2$

To investigate the dynamical stability of $B_5N_3O_2$, both the phonon dispersion calculations and molecular dynamics simulations were performed. The phonon dispersion (Fig. S1a, ESI†) shows that none of the acoustic vibrational modes is imaginary (both LA and TA are real) except the out-of-plane acoustic mode (ZA) mainly associated with long-range out-of-plane corrugations. The calculations of the phonon dispersion with different sizes of supercells show the trend toward vanishing of the imaginary part. The imaginary frequency of the ZA mode at the Γ-point (Fig. S1a, ESI†), comes from the lack of consideration of the rotational invariance.[38,39] Imposing the translational and rotational invariances, which is crucial for an accurate description of phonons in any 2D system, leads to vanishing of the imaginary frequency part of the ZA mode (Fig. S1b, ESI†). A detailed physical insight is presented in the ESI.†

Ab initio molecular dynamics (AIMD) simulations can show the origin of the imaginary mode in the phonon dispersion. Fig. 3 shows the oscillations of the total energy of $B_5N_3O_2$ at 600 and 1200 K. The energy is given with respect to the ground state (E_{min}) at 0 K. In Fig. 3 the side and top views of the atomic structure at 3 ps and 1200 K are shown. Both the energy

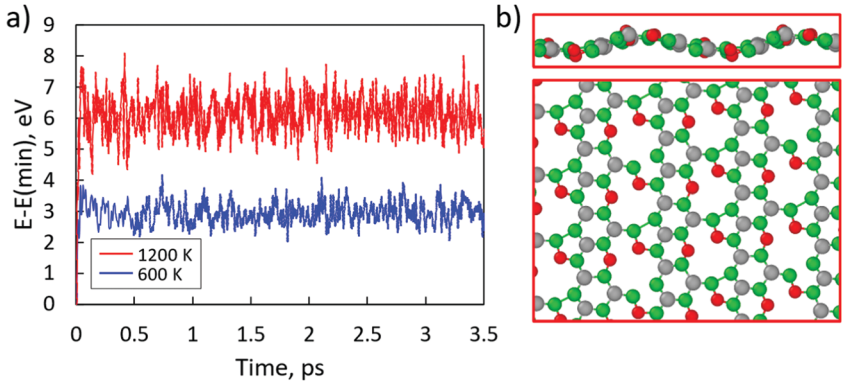

Fig. 3 Thermal stability of $B_5N_3O_2$ at finite temperatures. (a) Fluctuations of the potential energy (2 × 2 × 1 supercell) during the NVT *ab initio* MD simulations at 600 K (blue) and 1200 K (red). (b) Side and top views of the atomic structure at 3 ps and 1200 K. The boron, nitrogen, and oxygen atoms are shown in green, gray, and red, respectively.

oscillations and structure visualizations show dynamical stability of $B_5N_3O_2$. We assume that the out-of-plane corrugations that appeared because of the thermal motion (Fig. 3b, top panel) can be responsible for potential dynamical instability and the presence of imaginary modes in the phonon dispersion (the calculations of the phonon dispersion were carried out for an atomically flat structure). The AIMD simulations for other B–N–O structures predicted in this study are presented in Fig. S2 (ESI†).

In the B–N–O structures considered in this study, the number of various polygonal cycles rises as the oxygen concentration decreases. On the other hand, a decrease in the oxygen concentration should lead to dominance of the hexagonal structure of boron nitride, with oxygen replacing some nitrogen atoms or absorbing at the surface. In combination with the phonon dispersion results, this allows us to assert the stability of $B_5N_3O_2$.

Electronic and elastic properties of 2D boron oxynitride nanosheets

The calculation of the electronic properties of $B_5N_3O_2$ shows a decrease of the bandgap down to 3.0 eV based on PBE[27] calculations (Fig. S3a, ESI†), which is much smaller than for pure boron nitride and lower than that of the structures studied in previous works.[7] The main contribution in the top of valence bands comes from whole atoms B, N and O, but the bottom of conduction bands filled mainly by boron atoms similar to h-BN,[40] where the valence band is formed by a more electronegative nitrogen, while the conduction band is formed by less electronegative boron. The hybrid HSE06 functional expand the band gap value up to 4.4 eV (Fig. S3b, ESI†). The contribution of oxygen near the bandgap is equal to nitrogen, which indicates that the bandgap decrease is caused by the peculiarities of the two-dimensional crystal structure—the formation of non-hexagonal cycles in whole range of B–N–O structures (Fig. S4, ESI†). Additionally, to make a more accurate comparison, the Kubelka–Munk plot for $B_5N_3O_2$ was performed (Fig. S5 in the ESI†). The obtained direct optical band gap were estimated to be 2.9 eV and 2.5 eV for the longitudinal and transverse directions. It should be noted that the obtained greater value of the band gap in comparison with the experimental data are caused by the consideration of periodic BNO structures, while the band gap decrease is mainly caused by the presence of edge states due to the finite size of synthesized sample[7] as well as in pure h-BN, the formation of the edges leads to a decrease in the value of the band gap.[41] The results indicate the potential of using oxygen to obtain new semiconducting 2D materials based on the h-BN lattice.

Because the new materials are based on h-BN, we expected them to exhibit comparable mechanical properties. For all the predicted B–N–O structures, we estimated elastic constants using the stress–strain relations $\sigma_i = C_{ij}\eta_j$, where σ_i is ith component of the stress tensor, C_{ij} is the elastic tensor, η_j is ith component of the deformation tensor. The value of each elastic constant was determined as the slope of the obtained

Table 1 Elastic constants of 2D materials

	C_{11} (N m^{-1})	C_{12} (N m^{-1})	C_{22} (N m^{-1})	C_{44} (N m^{-1})
$B_5N_3O_2$	201.8	6.9	75.7	57.28
BNO (20 atom %)[7]	217.39	73.57	224.82	
BNO (10 atom %)[7]	235.34	65.957	240.29	
BC_2N(I)[7]	263.50	46.387	283.62	
BC_2N(II)[7]	292.73	51.744	283.25	
Graphene	342[43]			
	345[44]	64.1[48]		143.75[48]
	347.2[45]			
	348[46]			
	335[47]			
	351.6[48]			
h-BN	271[44]			
	291.3[45]			
	267[47]			
WS_2	148.47[48]	31.2[48]		58.63[48]
	137[49]	31.8[50]		
	146.5[50]	31.0[51]		
	144.0[51]			
	151.48[52]			
MoS_2	134.89[48]	32.03[48]		51.43[48]
	123[49]	33.0[50]		
	132.7[50]	32.6[51]		
	128.4[51]			
	138.12[52]			

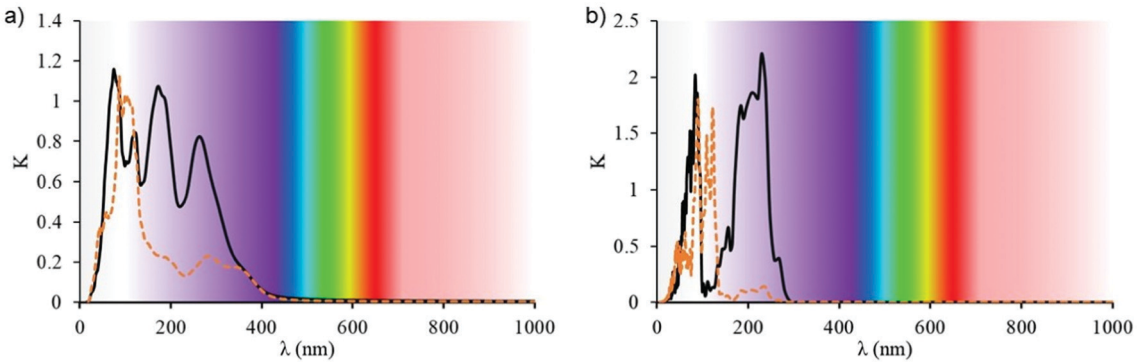

Fig. 4 Wavelength dependence of the extinction coefficient of (a) bulk $B_5N_3O_2$ and (b) bulk h-BN. Black and orange lines correspond to the longitudinal and transverse directions, respectively.

linear dependence: $C_{11} = \frac{\sigma_1}{\eta_1}$; $C_{22} = \frac{\sigma_2}{\eta_2}$; $C_{12} = \frac{\sigma_1}{\eta_2}$. The 2D linear elastic constants calculated for $B_5N_3O_2$ (C_{11} = 201.8 N m^{-1}, C_{22} = 75.7 N m^{-1}, and C_{12} = 6.9 N m^{-1}) are lower than those of h-BN[8–11] and graphene[8–10,12,13] but higher than those of transition metal dichalcogenides[11,14,15] (Table 1). The estimated values of the 2D elastic constants of the other B–N–O structures considered in this study are presented in Fig. S7 (ESI†). The new B–N–O nanostructures have more defective and less dense structure, and therefore lower elastic constants, than those with the oxygen concentrations of 20 and 10 atom % studied previously.[7] However, the B–N–O compositions described by Singh *et al.*[42] have a hexagonal h-BN structure with oxygen substituting some nitrogen atoms. The calculated elastic constant C_{11} of $B_5N_3O_2$ is comparable with that of the B– N– O composition with 20 atom % of oxygen and at the same time is higher than those of the monolayers of transition metal dichalcogenides MoS_2 and WS_2. Moreover, drastic changes in the atomic structure caused by the presence of oxygen may influence the electric response of B–N–O compositions under external mechanical deformation. The irregular geometry of $B_5N_3O_2$ may lead to a nonzero local dipole moment, which could play a significant role in the emergence or enhancement of piezoelectricity. We carried out *ab initio* calculations of the local dipole moments of the 5-member rings of $B_5N_3O_2$ and a part of the 6-member ring with oxygen (red and blue rectangles in Fig. S6, ESI†). Uncompensated local dipole moments of 6.21 D and 11.5 D were found in the 5- and 6-member rings, respectively. The directions of these local dipole moments are $\vec{n}$ = (0.54; 0.77; −0.32) and $\vec{n}$ = (0.04; 0.94; 0.31), respectively. The presence of nonzero local dipole moments of the individual components may indicate prospects for applications in the field of piezoelectric materials and requires a separate study. The 2D piezoelectric tensor of the B–N–O structures was also estimated (Table S1, ESI†).

Optical properties

Using the wavelength dependences of permittivity components, by means of the PBE functional[27] we estimated the extinction coefficient of $B_5N_3O_2$, which shows the capability to absorb electromagnetic radiation at different wavelengths. For polarized light propagating in both transverse and longitudinal directions to the oxynitride layers, the absorption peaks of $B_5N_3O_2$ are shifted closer to the visible range but are still located in the ultraviolet area (Fig. 4a) in comparison with pure h-BN (Fig. 4b). In the ultraviolet region with λ = 200–400 nm, the absorption of the longitudinally propagating radiation is significantly higher than that of the perpendicularly propagating radiation. We also carried out the calculations of dependence of the extinction coefficient on the wavelength by applying the HSE06 hybrid functional[53] (see Fig. S6 in the ESI†). The obtained data states about the larger absorption in the ultraviolet region with λ = 200–400 nm in comparison with h-BN.

IV. Conclusions

Using the USPEX evolutionary algorithm, we predicted the structures of the $B_xN_yO_z$ two-dimensional nanoscale arrangements. Along with compositions in which some nitrogen atoms are replaced by oxygen, unique B–N–O structures were found. The experimental data on the synthesis of boron oxynitride suggests a larger interplanar distance than in pure h-BN. Among the structures we predicted, $B_5N_3O_2$ has the oxygen concentration similar to that of an experimentally obtained composition and a similarly expanded interplanar distance. This may indicate that its structure is probably different from the hexagonal arrangement of h-BN with incorporated oxygen atoms that can be observed experimentally. The elastic constants of the predicted compositions are comparable with the mechanical properties of boron nitride. We assumed that the incorporation of oxygen atoms into the structure of 2D BN can cause local dipole moments which might improve its piezoelectric properties. The calculated electronic structure shows a decrease in the bandgap caused by the addition of oxygen, which also leads to a red shift of absorption peaks toward near UV region. Our results explain the puzzling properties of oxidized BN sheets determined in previous experiments.

Conflicts of interest

There are no conflicts to declare.

Acknowledgements

We thank E. V. Sukhanova for a fruitful discussion and assistance in carrying out HSE calculations. D. G. K. acknowledges the grant from the President of the Russian Federation for the support of young PhD scientists (MK-3120.2021.1.2) and for the financial support of the prediction of novel B– N– O structures as promising materials with high piezoelectric coefficients. D. G. K., V. A. D. and Z. I. P. thank the Russian Science Foundation (project No. 21-73-10238) for the financial support of the DFT calculations of the local dipole moments of defected BN structures. The authors express their gratitude to the Joint Supercomputer Center of the Russian Academy of Sciences and the Information Technology Centre of Novosibirsk State University for providing access to cluster computational resources.

References

1 L. Stagi, J. Ren and P. Innocenzi, From 2-D to 0-D Boron Nitride Materials, The Next Challenge, *Materials*, 2019, **12**, 3905.
2 S. Yu, X. Wang, H. Pang, R. Zhang, W. Song, D. Fu, T. Hayat and X. Wang, Boron nitride-based materials for the removal of pollutants from aqueous solutions: A review, *Chem. Eng. J.*, 2018, **333**, 343–360.
3 J. Dai, X. Wu, J. Yang and X. C. Zeng, Unusual Metallic Microporous Boron Nitride Networks, *J. Phys. Chem. Lett.*, 2013, **4**, 3484–3488.
4 L. Vel, G. Demazeau and J. Etourneau, Cubic boron nitride: synthesis, physicochemical properties and applications, *Mater. Sci. Eng., B*, 1991, **10**, 149–164.
5 R. R. Wills, Wurtzitic boron nitride—a review, *Int. J. High Technol. Ceram.*, 1985, **1**, 139–153.
6 Q. Weng, X. Wang, X. Wang, Y. Bando and D. Golberg, Functionalized hexagonal boron nitride nanomaterials: emerging properties and applications, *Chem. Soc. Rev.*, 2016, **45**, 3989–4012.
7 Q. Weng, D. G. Kvashnin, X. Wang, O. Cretu, Y. Yang, M. Zhou, C. Zhang, D.-M. Tang, P. B. Sorokin, Y. Bando and D. Golberg, Tuning of the Optical, Electronic, and Magnetic Properties of Boron Nitride Nanosheets with Oxygen Doping and Functionalization, *Adv. Mater.*, 2017, **29**, 1700695–1700712.
8 C. Elias, P. Valvin, T. Pelini, A. Summerfield, C. J. Mellor, T. S. Cheng, L. Eaves, C. T. Foxon, P. H. Beton, S. V. Novikov, B. Gil and G. Cassabois, Direct band-gap crossover in epitaxial monolayer boron nitride, *Nat. Commun.*, 2019, **10**, 2639.
9 X. Blase, A. Rubio, S. G. Louie and M. L. Cohen, Quasiparticle band structure of bulk hexagonal boron nitride and related systems, *Phys. Rev. B: Condens. Matter Mater. Phys.*, 1995, **51**, 6868–6875.
10 F. Paleari, T. Galvani, H. Amara, F. Ducastelle, A. Molina-Sánchez and L. Wirtz, Excitons in few-layer hexagonal boron nitride: Davydov splitting and surface localization, *2D Mater.*, 2018, **5**, 045017.
11 G. Cassabois, P. Valvin and B. Gil, Hexagonal boron nitride is an indirect bandgap semiconductor, *Nat. Photonics*, 2016, **10**, 262–266.
12 R. Schuster, C. Habenicht, M. Ahmad, M. Knupfer and B. Büchner, Direct observation of the lowest indirect exciton state in the bulk of hexagonal boron nitride, *Phys. Rev. B*, 2018, **97**, 041201.
13 J. Ren, L. Stagi, C. M. Carbonaro, L. Malfatti, M. F. Casula, P. C. Ricci, A. E. D. R. Castillo, F. Bonaccorso, L. Calvillo, G. Granozzi and P. Innocenzi, Defect-assisted photoluminescence in hexagonal boron nitride nanosheets, *2D Mater.*, 2020, **7**, 045023.
14 L. Weston, D. Wickramaratne, M. Mackoit, A. Alkauskas and C. G. Van de Walle, Native point defects and impurities in hexagonal boron nitride, *Phys. Rev. B*, 2018, **97**, 214104.
15 J. Ren, L. Malfatti, S. Enzo, C. M. Carbonaro, L. Calvillo, G. Granozzi and P. Innocenzi, Boron oxynitride two-colour fluorescent dots and their incorporation in a hybrid organic-inorganic film, *J. Colloid Interface Sci.*, 2020, **560**, 398–406.
16 L. A. Silva, S. C. Guerini, V. Lemos and J. M. Filho, Electronic and Structural Properties of Oxygen-Doped BN Nanotubes, *IEEE Trans. Nanotechnol.*, 2006, **5**, 517–522.
17 J. Wu and W. Zhang, Tuning the magnetic and transport properties of boron-nitride nanotubes via oxygen-doping, *Solid State Commun.*, 2009, **149**, 486–490.
18 G. Gou, B. Pan and L. Shi, The Nature of Radiative Transitions in O-Doped Boron Nitride Nanotubes, *J. Am. Chem. Soc.*, 2009, **131**, 4839–4845.
19 L. Liu, T.-K. Sham and W. Han, Investigation on the electronic structure of BN nanosheets synthesized via carbon-substitution reaction: the arrangement of B, N, C and O atoms, *Phys. Chem. Chem. Phys.*, 2013, **15**, 6929–6934.
20 O. L. Krivanek, M. F. Chisholm, V. Nicolosi, T. J. Pennycook, G. J. Corbin, N. Dellby, M. F. Murfitt, C. S. Own, Z. S. Szilagyi, M. P. Oxley, S. T. Pantelides and S. J. Pennycook, Atom-by-atom structural and chemical analysis by annular dark-field electron microscopy, *Nature*, 2010, **464**, 571–574.
21 B. C. Revard, W. W. Tipton, A. Yesypenko and R. G. Hennig, Grand-canonical evolutionary algorithm for the prediction of two-dimensional materials, *Phys. Rev. B*, 2016, **93**, 054117.
22 A. R. Oganov and C. W. Glass, Crystal structure prediction using ab initio evolutionary techniques: Principles and applications, *J. Chem. Phys.*, 2006, **124**, 244704.
23 Q. Zhu, L. Li, A. R. Oganov and P. B. Allen, Evolutionary method for predicting surface reconstructions with variable stoichiometry, *Phys. Rev. B: Condens. Matter Mater. Phys.*, 2013, **87**, 195317.
24 A. O. Lyakhov, A. R. Oganov, H. T. Stokes and Q. Zhu, New developments in evolutionary structure prediction algorithm USPEX, *Comput. Phys. Commun.*, 2013, **184**, 1172–1182.
25 P. Hohenberg and W. Kohn, Inhomogeneous Electron Gas, *Phys. Rev.*, 1964, **136**, B864–B871.
26 W. Kohn and L. J. Sham, Self-Consistent Equations Including Exchange and Correlation Effects, *Phys. Rev.*, 1965, **140**, A1133–A1138.

27 J. P. Perdew, K. Burke and M. Ernzerhof, Generalized Gradient Approximation Made Simple, *Phys. Rev. Lett.*, 1996, **77**, 3865–3868.
28 G. Kresse and J. Hafner, Ab initio molecular dynamics for liquid metals, *Phys. Rev. B: Condens. Matter Mater. Phys.*, 1993, **47**, 558–561.
29 G. Kresse and J. Hafner, Ab initio molecular-dynamics simulation of the liquid-metal-amorphous-semiconductor transition in germanium, *Phys. Rev. B: Condens. Matter Mater. Phys.*, 1994, **49**, 14251–14269.
30 G. Kresse and J. Furthmüller, Efficient iterative schemes for ab initio total-energy calculations using a plane-wave basis set, *Phys. Rev. B: Condens. Matter Mater. Phys.*, 1996, **54**, 11169–11186.
31 G. Kresse and J. Furthmüller, Efficiency of ab-initio total energy calculations for metals and semiconductors using a plane-wave basis set, *Comput. Mater. Sci.*, 1996, **6**, 15–50.
32 S. Grimme, J. Antony, S. Ehrlich and H. Krieg, A consistent and accurate ab initio parametrization of density functional dispersion correction (DFT-D) for the 94 elements H-Pu, *J. Chem. Phys.*, 2010, **132**, 154104.
33 A. Togo and I. Tanaka, First principles phonon calculations in materials science, *Scr. Mater.*, 2015, **108**, 1–5.
34 M. Gajdoš, K. Hummer, G. Kresse, J. Furthmüller and F. Bechstedt, Linear optical properties in the projector-augmented wave methodology, *Phys. Rev. B: Condens. Matter Mater. Phys.*, 2006, **73**, 045112.
35 S. Nosé, A unified formulation of the constant temperature molecular dynamics methods, *J. Chem. Phys.*, 1984, **81**, 511–519.
36 W. G. Hoover, Canonical dynamics: Equilibrium phase-space distributions, *Phys. Rev. A: At., Mol., Opt. Phys.*, 1985, **31**, 1695–1697.
37 R. Zhang, Z. Li and J. Yang, Two-Dimensional Stoichiometric Boron Oxides as a Versatile Platform for Electronic Structure Engineering, *J. Phys. Chem. Lett.*, 2017, **8**, 4347–4353.
38 Y. D. Kuang, L. Lindsay, S. Q. Shi and G. P. Zheng, Tensile strains give rise to strong size effects for thermal conductivities of silicene, germanene and stanene, *Nanoscale*, 2016, **8**, 3760–3767.
39 A. S. Nissimagoudar, A. Manjanath and A. K. Singh, Diffusive nature of thermal transport in stanene, *Phys. Chem. Chem. Phys.*, 2016, **18**, 14257–14263.
40 M. Topsakal, E. Aktürk and S. Ciraci, First-principles study of two- and one-dimensional honeycomb structures of boron nitride, *Phys. Rev. B: Condens. Matter Mater. Phys.*, 2009, **79**, 115442–115453.
41 A. Yamanaka and S. Okada, Energetics and Electronic Structure of h-BN Nanoflakes, *Sci. Rep.*, 2016, **6**, 30653.
42 R. S. Singh, R. Yingjie Tay, W. Leong Chow, S. Hon Tsang, G. Mallick and E. H. Tong Teo, Band gap effects of hexagonal boron nitride using oxygen plasma, *Appl. Phys. Lett.*, 2014, **104**, 163101.
43 C. Lee, X. Wei, J. W. Kysar and J. Hone, Measurement of the Elastic Properties and Intrinsic Strength of Monolayer Graphene, *Science*, 2008, **321**, 385–388.
44 K. N. Kudin, G. E. Scuseria and B. I. Yakobson, C_2F, BN, and C nanoshell elasticity from ab initio computations, *Phys. Rev. B: Condens. Matter Mater. Phys.*, 2001, **64**, 10.
45 Q. Peng, A. R. Zamiri, W. Ji and S. De, Elastic properties of hybrid graphene/boron nitride monolayer, *Acta Mech.*, 2012, **223**, 2591–2596.
46 X. Wei, B. Fragneaud, C. A. Marianetti and J. W. Kysar, Nonlinear elastic behavior of graphene: Ab initio calculations to continuum description, *Phys. Rev. B: Condens. Matter Mater. Phys.*, 2009, **80**, 205407.
47 M. Topsakal, S. Cahangirov and S. Ciraci, The response of mechanical and electronic properties of graphane to the elastic strain, *Appl. Phys. Lett.*, 2010, **96**, 091912.
48 Z. Fan, Z. Wei-Bing and T. Bi-Yu, Electronic structures and elastic properties of monolayer and bilayer transition metal dichalcogenides MX 2 (M = Mo, W; X = O, S, Se, Te): A comparative first-principles study, *Chin. Phys. B*, 2015, **24**, 097103.
49 K. Liu, Q. Yan, M. Chen, W. Fan, Y. Sun, J. Suh, D. Fu, S. Lee, J. Zhou, S. Tongay, J. Ji, J. B. Neaton and J. Wu, Elastic Properties of Chemical-Vapor-Deposited Monolayer MoS2, WS2, and Their Bilayer Heterostructures, *Nano Lett.*, 2014, **14**, 5097–5103.
50 D. Çakır, F. M. Peeters and C. Sevik, Mechanical and thermal properties of h-MX2 (M = Cr, Mo, W; X = O, S, Se, Te) monolayers: A comparative study, *Appl. Phys. Lett.*, 2014, **104**, 203110.
51 Q. Peng and S. De, Outstanding mechanical properties of monolayer MoS2 and its application in elastic energy storage, *Phys. Chem. Chem. Phys.*, 2013, **15**, 19427–19437.
52 C. Ataca, H. Sahin and S. Ciraci, Stable, Single-Layer MX2 Transition-Metal Oxides and Dichalcogenides in a Honeycomb-Like Structure, *J. Phys. Chem. C*, 2012, **116**, 8983–8999.
53 A. V. Krukau, O. A. Vydrov, A. F. Izmaylov and G. E. Scuseria, Influence of the exchange screening parameter on the performance of screened hybrid functionals, *J. Chem. Phys.*, 2006, **125**, 224106.

